Astron. Astrophys. 341, 675–682 (1999)

ASTRONOMY AND ASTROPHYSICS

AGN polarization models

S. Wolf[1] **and Th. Henning**[2]

[1] Thüringer Landessternwarte Tautenburg, Sternwarte 5, D-07778 Tautenburg, Germany
[2] Astrophysikalisches Institut und Universitäts-Sternwarte (AIU), Schillergässchen 3, D-07745 Jena, Germany

Received 31 July 1998 / Accepted 4 November 1998

Abstract. We present model calculations for the scattered flux and polarization of nuclear radiation having in mind the AGN unification scheme. It is our aim to survey the influence of several model parameters, especially, the influence of the torus. Additionally, we considerably improved present models, for instance by including multiple instead of single scattering.

For these purposes, we developed a Monte-Carlo radiative transfer code for both electron and dust scattering (Thomson and Rayleigh/Mie scattering). Irradiation from a point-like source can be treated as well as extended anisotropic radiation sources and dust re-emission.

We found that the observed wavelength dependence of the linear polarization of some AGNi can be explained by dust scattering in optically thin cones, whereby the additional presence of electrons increases the absolute amount of polarization. The torus geometry and density profile as well as the thermal dust reemission also influence the polarization degree. Multiple scattering in the cones was found to be important for optical depths above ≈ 0.1.

Key words: galaxies: Seyfert – galaxies: active – radiative transfer – scattering – polarization

1. Introduction

The investigation of AGNi by polarimetric measurements provides an already well-established basis for deriving their geometrical structure. The available results from observations of AGNi show that the behaviour of polarization fits in principle to the current unified model of Seyfert galaxies, as proposed by Antonucci & Miller (1985). Their model is based on the assumption that all Seyfert galaxies host a Seyfert 1 type nucleus surrounded by a geometrically and optically thick torus which obscures our view of the nuclear regions for the type 2 Seyferts but not for the Seyfert 1 galaxies.

Recently, the polarization has been discussed to originate from light scattering on electrons and/or dust grains (Thomson and/or Rayleigh/Mie scattering) and dichroic extinction (see, e.g., Brindle et al. 1990, Miller & Goodrich 1990, Goodrich & Miller 1994, Young et al. 1995, Manzini & di Serego Alighieri 1996, Kartje 1995). While the scattering mechanism and the resulting polarization are already well-studied in connection with other astrophysical objects (e.g., young stellar objects), the spatial distribution of scatterers in AGNi – and therefore the AGNi structure – is a still unresolved problem.

During the last decade a broad spectrum of AGN models – particularly for Seyfert galaxies – has been developed to explain both their flux and polarization features. The most simple kind of models consists of two opposite cones with a density distribution of scatterers following a power law or a constant density (see, e.g., Miller & Goodrich 1990, Manzini & di Serego Alighieri 1996). The nuclear radiation is emitted along these diametrically opposed cones, while the torus which is expected to provide this collimation is neglected. Although this model has many drawbacks (e.g., no multiple scattering, influence of torus geometry and dust/electron distribution neglected, only point-like central radiation source treated – no thermal reemission from dusty tori), a fundamental understanding of the characteristic behaviour and the amount of polarization degree in both types of Seyfert galaxies can be derived. The torus geometry has been studied primarily with respect to the infrared emission of AGNi (see, e.g., Pier & Krolik 1992, 1993, Efstathiou & Rowan-Robinson 1995 – hereafter ER95, Efstathiou et al. 1995, Manske et al. 1998).

In this paper we consider the polarization arising from various model geometries. Firstly, we give a short description of the general model geometry (Sect. 2.1) and our Monte-Carlo radiative transfer code (Sect. 2.2). Secondly, we compare results of our code with analytic solutions for two standard configurations (Sect. 3.1). Thirdly, we investigate the multiple scattering effect (Sect. 3.2) and the influence of the torus as well as extended radiation sources on the observable polarization (Sects. 3.3, 3.4) considering electron and/or dust scattering.

2. The model

2.1. General configuration

Our AGN models (see Fig. 1) consist of a torus (1, optically thick), an outer region (2, optically thin), and an inner region (3, optically thin). There can be both electrons and dust grains separated or mixed in all 3 regions. The radiation was assumed to

Send offprint requests to: S. Wolf (wolf@tls-tautenburg.de)

originate from a point-like central source, the – extended – inner region, or the inner surface of the torus. The exact geometry and parameter set depends on the particular model (see Sect. 3).

2.2. The simulation of the radiative transfer

2.2.1. The code

For the simulation of the radiative transfer we developed a Monte-Carlo radiative transfer code. It is based on the code of Fischer et al. (1994) which was developed for the simulation of polarization maps of pre-main sequence objects. The radiation has been partitioned into so-called weighted test photons. Every test photon is characterized by its wavelength and its Stokes vector $(I, Q, U, V)_{\rm T}$ which becomes modified due to scattering and absorption. Both intensity and polarization maps as well as the integrated values can be derived from the Stokes vectors of the test photons. Electron and dust scattering (Thomson and Rayleigh/Mie scattering) can be treated. It is possible to separate and to mix both electrons and dust grains, spatially.

2.2.2. The dust

Beside electron scattering, we performed our calculations with 2 different grain populations – a diffuse ISM population ("ISM", radii between 0.005 and 0.25 μm) and a population with only larger grains ("LAR", radii between 0.1 and 1 μm). We used the optical data of Draine & Lee (1984). For both populations the grains are distributed with a number density $n(a) \propto a^{-3.5}$ (a is the radius of the spherical dust grains). We considered a dust mixture of 62.5% "astronomical" silicate and 37.5% graphite (25% – **E** oscillates parallel to the graphite plane, 12.5% – **E** oscillates perpendicular to the graphite plane) as the basis for the optical dust data. In Fig. 2 the albedo for both dust populations is shown for the wavelength range between 0.050 μm and 1.000 μm.

As grains with different radii or of different materials have various cross sections ($C_{\rm sca}$, $C_{\rm ext}$) and elements of the scattering matrix ($\hat{S}$), these grain parameters are expressed for a mixture by the corresponding "representative" values $\langle C_{\rm sca}\rangle$, $\langle C_{\rm ext}\rangle$, and $\left\langle \hat{S} \right\rangle$:

$$\langle C_{\rm sca}\rangle = \sum_{i=1}^{w} \int_{a_{\rm min}}^{a_{\rm max}} g_i(a) C_{{\rm sca}_i}(a) da, \tag{1}$$

$$\langle C_{\rm ext}\rangle = \sum_{i=1}^{w} \int_{a_{\rm min}}^{a_{\rm max}} g_i(a) C_{{\rm ext}_i}(a) da, \tag{2}$$

$$\left\langle \hat{S} \right\rangle = \sum_{i=1}^{w} \int_{a_{\rm min}}^{a_{\rm max}} g_i(a) \hat{S}_i(a) da \tag{3}$$

With regard to the optical effect of each component of the dust mixture, the weight $g_i(a)$ depends on the abundance of the i-th material component (w components are present) and on the size distribution of the dust particles (in the range between the smallest $a_{\rm s}^{(i)}$ and the largest $a_{\rm l}^{(i)}$ radii) of each component. Here, we have normalized $g_i(a)$ so that

$$\sum_{i=1}^{w} \int_{a_{\rm min}}^{a_{\rm max}} g_i(a) da = 1 \tag{4}$$

The "representative" value of the albedo can be calculated as follows:

$$\langle albedo\rangle = \frac{\langle C_{\rm sca}\rangle}{\langle C_{\rm ext}\rangle} \tag{5}$$

Firstly, we consider only electron scattering in the lobes. After that we will also discuss scattering by dust grains.

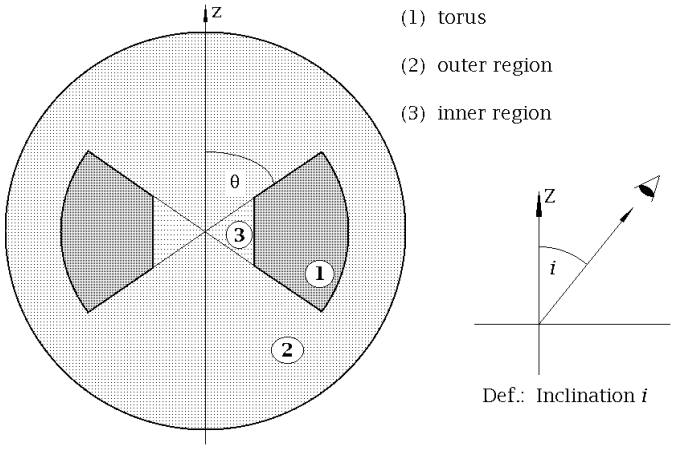

Fig. 1. General model geometry (see text)

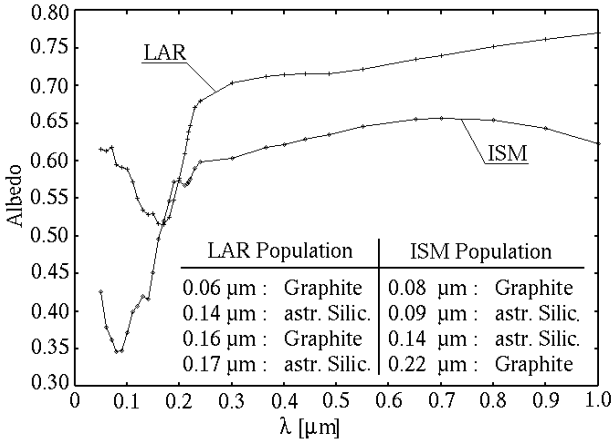

Fig. 2. Absorption bands of the ISM and LAR population. The dots mark the wavelengths at which the transfer of radiation was computed.

3. Results

3.1. Comparison with previous calculations

3.1.1. Plane-parallel atmosphere

While the dust scattering routines of our code are already well-tested (e.g., Fischer et al. 1994, 1996; Wolf et al. 1998), the new electron scattering part still had to be checked. For this, we calculated the polarization arising from electron scattering

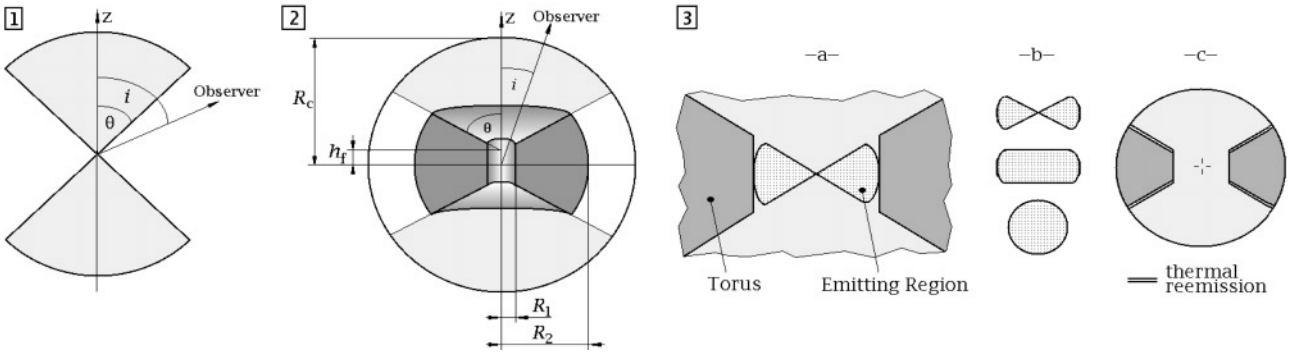

Fig. 3.
1. Model for comparison with the analytic solution of Brown & McLean (BM, see Sect. 3.1.2)
2. Geometry of the model treated in this paper (see Sect. 3)
3. Configurations of extended radiation sources (see Sect. 3.4)
   (a) Configuration of the extended central radiation source.
   (b) Investigated radiation sources of different shape.
   (c) Thermally re-emitting surfaces of the dusty torus.

within a plane-parallel slab, and compared our results with those calculated with an analytic approach by Chandrasekhar (1960). For a more detailed description of this test, we refer to Wood et al. (1996) who used the same model to test their code. Our results agree with the expected values.

3.1.2. Formalism of Brown & McLean

Brown & McLean (1977, hereafter: BM) studied the polarization by axisymmetric, optically thin distributions of scatterers, centred on the central radiation source but otherwise of entirely general density distribution and at an arbitrary inclination. They showed that all such envelopes produce a polarization P of the scattered light, given by

$$P = sin^2 i/(2\alpha + sin^2 i) \quad (6)$$

with $\alpha = (1+\gamma)/(1-3\gamma)$. Here the quantity γ is a "shape factor", defined by the ratio of two moments (integrals) of the density distribution function in spherical coordinates. It is related to the oblateness (or prolateness) of the envelope.

The most simple Seyfert 2 AGN polarization model is based on "cones" (segments with half opening angle θ, see Fig. 3.1) seen under intermediate inclinations i ($\theta \leq i \leq 180° - \theta$). For $i \leq \theta$ we can look into the nucleus (classification: Seyfert 1). Following Miller & Goodrich (1990, hereafter: MG90), the value of α in the BM formalism for this model geometry is given by

$$\alpha = -(4 + \mu + \mu^2)/(3\mu + 3\mu^2), \quad (7)$$

where $\mu = \cos\theta$.

We simulated the radiative transfer in this configuration. To get results comparable with the analytic solution of BM, we defined a low optical depth in the electron-filled cones ($\tau_V(z)$=0.2; optical depth along the z-axis seen from the central source; electron density $n(e^-)$=const.) and neglected multiply scattered photons. The radiation from the point-like central source was limited to the emission into the cones. Thus, only scattered radiation can leave the configuration for $\theta \leq i \leq 180° - \theta$. Fig. 4 shows the excellent agreement between the analytic solution of BM and our results.

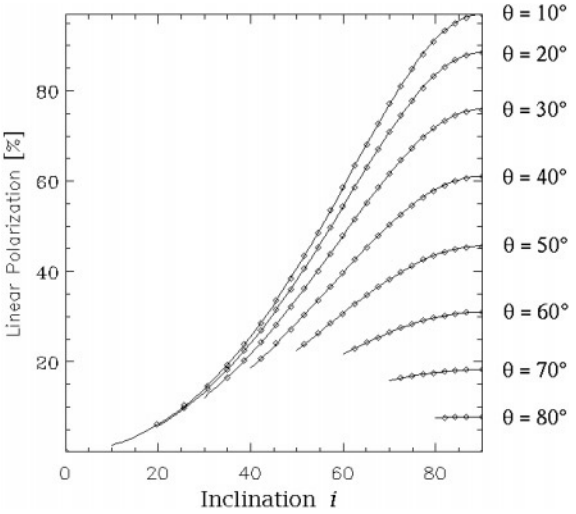

Fig. 4. Polarization from scattering in optically thin cones, seen under intermediate inclinations ($\theta \leq i \leq 180° - \theta$). Solid lines: analytic solution of BM (see text); dotted lines: Monte-Carlo simulation results

3.2. Multiple scattering effect

The BM formalism applied to the model geometry described in Sect. 3.1.2 or similar geometries provides the basis for many AGN polarization models and many other single-scattering models for Thomson scattering in various axisymmetric optically thin envelopes illuminated by a point source (see, e.g., G 2 oodrich & Miller 1994, Miller et al. 1991, MG90). A fundamental drawback of this analytic solution is the inability to describe the influence of multiple scattering. The common argument for neglecting multiple scattering are observational hints

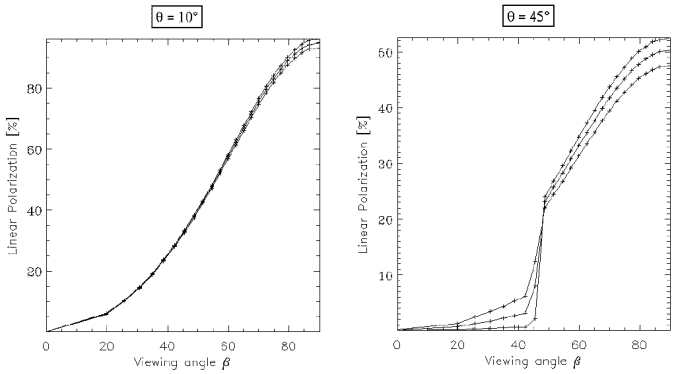

Fig. 5. Polarization from multiple scattering in cones. $\tau_{\rm V} = 0.1, 0.5, 1.0$. The arrows show the shift direction of the curves for increasing optical depth τ_V along the z-axis

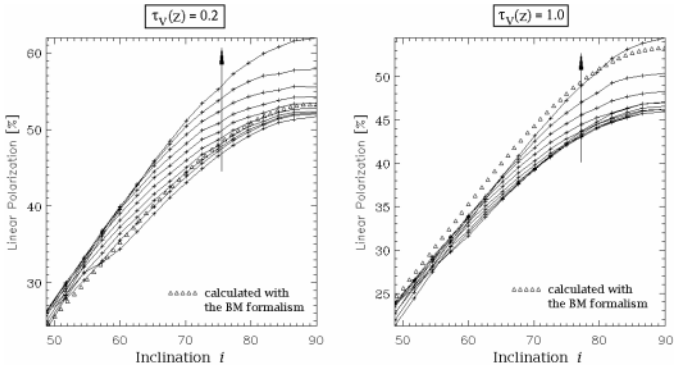

Fig. 6. Polarization for different torus radii. $\theta = 45°$, $\tau_{\rm V}(\rm torus)$=100, dust population in the torus: LAR, $R_1 \leq R_2/10$, λ=550nm. The arrows show the shift direction of the curves for increasing relative sizes of the torus $R_2/R_{\rm c}$ ($R_2/R_{\rm c}$ = 0.01, 0.1, 0.2, 0.3, . . ., 0.9, 1.0)

on optically thin electron scattering in cones of Seyfert 2's. The electron scattering optical depth $\tau_V(z)$ in these objects is expected to be less than unity (e.g., $\tau = 0.04$ in NGC 1068, Miller et al. 1991; see also MG90, Young et al. 1995, Efstathiou et al. 1995, Kishimoto 1996).

In Fig. 5 the influence of multiple scattering on the linear polarization degree $P_{\rm l}$ is shown both for the case of Seyfert 1's ($i < \theta$) and Seyfert 2's ($\theta < i < 180° - \theta$). For $\theta = 45°$, $P_{\rm l}$ changes noticeably even though the optical depth does not exceed 1. In the Seyfert 1 case, the degree of linear polarization is very small ($P_{\rm l} < 1\%$) for low optical depths (Fig. 5, $\tau_{\rm V}(z)$=0.2) because of substantial contribution of non-scattered and, therefore, unpolarized radiation. The polarization degree $P_{\rm l}$ increases with increasing optical depth following the decrease of the intensity of the direct non-scattered radiation. For $\theta < i < 180° - \theta$ the increasing scattering probability leads to the decrease of $P_{\rm l}$.

3.3. Influence of the torus

3.3.1. Influence of the torus size

Current unified theories of AGNi and quasars assume the continuum source and broad-line region to be surrounded by a geometrically and optically thick torus of obscuring material. As the most fundamental consequence, this leads to an understanding of the phenomenological differences between Seyfert 1's and 2's (see, e.g., Lawrence 1987, Antonucci 1993).

The collimation of the central source radiation into opposite cones was treated artificially in the previous models by emitting photons only into the cones (see Sects. 3.1.2, 3.2). Similar AGNi models were developed by Young et al. (1995) and Manzini & di Serego Alighieri (1996). In contrast to this basic approach, the assumption of radiation collimation due to a torus seems to be more realistic.

In our following model, the torus geometry is defined by 3 parameters: the inner radius R_1, the outer radius R_2, and the torus height $h_{\rm f}$ (see Fig. 3.2). The radius of the cones is $R_{\rm c}$. The – optically thick – torus (equatorial optical depth $\tau_{\rm V}(\rm torus)$) is filled with dust. Observational hints for this assumption are:

- strong IR emission over a wide wavelength range ($3 . . . 10$ μm)
- the steep fall of the spectral energy distribution between about 100 μm and the mm wavelength range in the case of radio-quiet AGNi being regarded as an evidence for a thermal origin of the IR emission (Chini et al. 1989, Lawrence et al. 1991)
- an intensity minimum at about 1 μm (Sanders et al. 1989) and a bump peaking at $3 - 5$ μm (Edelson & Malkan 1986, Robson et al. 1986) as indicators for hot dust with a sublimation temperature of 1000. . .1500 K.

The behaviour of $P_{\rm l}$, depending on the relative size of the torus $R_2/R_{\rm c}$, is shown in Fig. 6 for $\theta = 45°$ (for the illustration of the structure of the configuration Fig. 7 gives the intensity and polarization maps for $\theta = 45°, 80°$ and $R_2/R_{\rm c} = 0.4$). Increasing the outer radius R_2 of the torus, the screened inner region around the central source is enlarged. Because of the following two reasons the net polarization of light seen under an inclination of $\theta < i < 180° - \theta$ increases with increasing torus size (*screening effect*): Firstly, we are seeing the cone whose inner portion is cut linearly, determined by the torus edge and our line of sight. Therefore, the inner boundary of the visible part of the cone is not a concentric surface. Secondly, the polarization of the scattered light arising from the cones increases with increasing projected distance from the central source. Thus, the screening effect is strengthened if the electron density increases towards the central radiation source. Then, the percentage of the less polarized radiation arising from the inner regions of the cones increases because of the increasing scattering probability. This implies that the net polarization decreases. This can be "prevented" by the screening effect described above (see Fig. 8). Because most of the AGN polarization models, based on electron/dust scattering in cones, assume a power law to describe the density profile ($n(e^-) \propto r^{-|\alpha|}$, where r is the distance from the central source, $\alpha = const.$; see, e.g., Efstathiou et al. 1995, Manzini & di Serego 1996, Mulchaey et al. 1996), it is necessary to consider this effect. For low optical depths ($\tau_{\rm V}(z) \ll 1$) the BM formalism can be applied if the torus is small compared

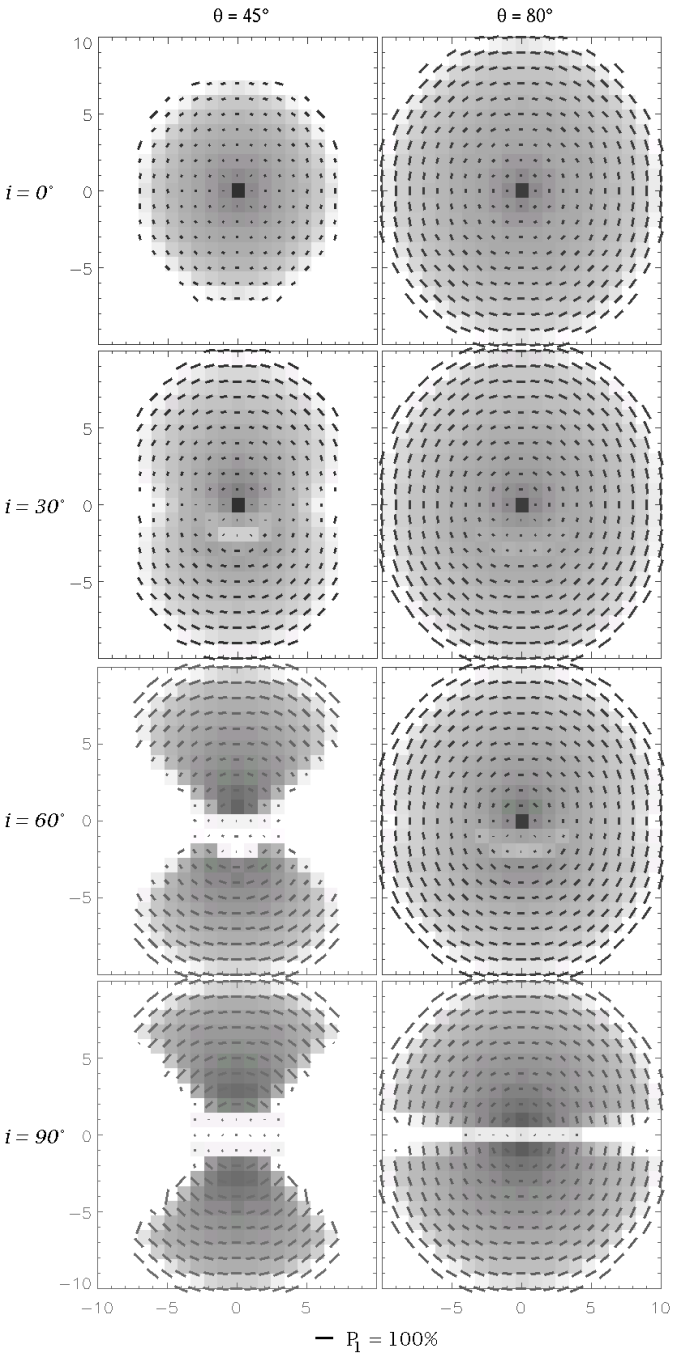

Fig. 7. Intensity maps with overlayed polarization pattern for the configuration described in Sect. 3.3.1 seen under different inclination angles i (see also Fig. 3). Half opening angle of the torus $\theta = 45°, 80°$; $\tau_{\rm V}(z)$=1.0, $\tau_{\rm V}(\rm torus)$=1000, dust population in the torus: ISM, λ=550nm

to the cone size (see Fig. 6, $\tau_{\rm V}(z)$=0.2). Because the multiple scattering and the screening represent two effects running in opposite directions, the best agreement with the BM solution for higher optical depths is found at larger torus radii (see Fig. 6, $\tau_{\rm V}(z)$=1.0).

For $i < \theta$ (Seyfert 1), there is no screening effect. With the exception of multiple scattering in the cones, any difference to the BM solution must be caused by scattering on the torus surface. The influence of this dust scattering on the polarization was found to be marginal because electron scattering produces much higher degrees of polarization than dust scattering in an equivalent configuration (same geometry and optical depth). Furthermore, the scattering by dust grains attenuates the radiation by absorption in contrast to electron scattering, where the intensity of the (test) photons is conserved. Therefore, the contribution of the dust-scattered photons to the net flux and net polarization is only small.

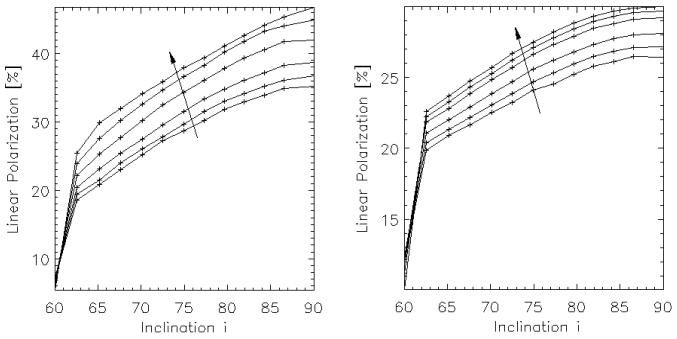

Fig. 8. "Enforced" screening effect in the case of a electron density in the cones following the power law $n(e^-) \propto r^{-|\alpha|}$. *Left:* Torus screens the inner region of the cones. *Right:* No torus. The less polarized radiation arising from the inner optically thicker regions dominates the net polarization. The arrows show the shift direction of the curves due to increasing α ($\alpha = 0, 0.2, 0.5, 1.0, 1.5, 2.0$).

The polarization shows only a weak wavelength dependence. This reflects the small influence of dust scattering in the torus, too: For R_1/R_2=0.05, θ=45°, $\tau_{\rm V}(\rm torus)$=1000, and $\tau_{\rm V}(z)$=1 we calculated the degree of linear polarization for λ=0.05...1 μm. We found $\Delta_{\max}P \approx 2\%$ for $\theta < i < (180° - \theta)$ and $\Delta_{\max}P \ll 1\%$ for $i < \theta$, where $\Delta_{\max}P$ is the difference between the maximum and the minimum polarization over the wavelength range. There is no significant dependence of the polarization on the kind of dust population in the torus (LAR/ISM, see Sect. 2.2.2).

Finally, if we assume electrons to be the dominant scatterers even on the torus surface, the influence of the photons being scattered on the surface increases. Because these photons have been scattered at least two times in the Seyfert 2 case before they reach the observer, the net polarization decreases (see Fig. 9).

3.3.2. Several characteristics of large torus models

The influence of the torus on the radiative transfer can be studied best, if it is large compared to the cone size ($R_2/R_{\rm c} \Rightarrow 1$). Models with large torus sizes were suggested by Pier & Krolik (1992), ER95, and Efstathiou et al. (1995). In the following, we discuss the influence of different parameters for the "large torus case".

Firstly, we investigated the influence of the inner torus radius R_1 for $\theta = 45°$ and 80° in the range $R_1/R_2 = 0.01, 0.02, \ldots, 0.10$. Both, the change of the polarization and of the intensity were negligible ($\ll 1\%$).

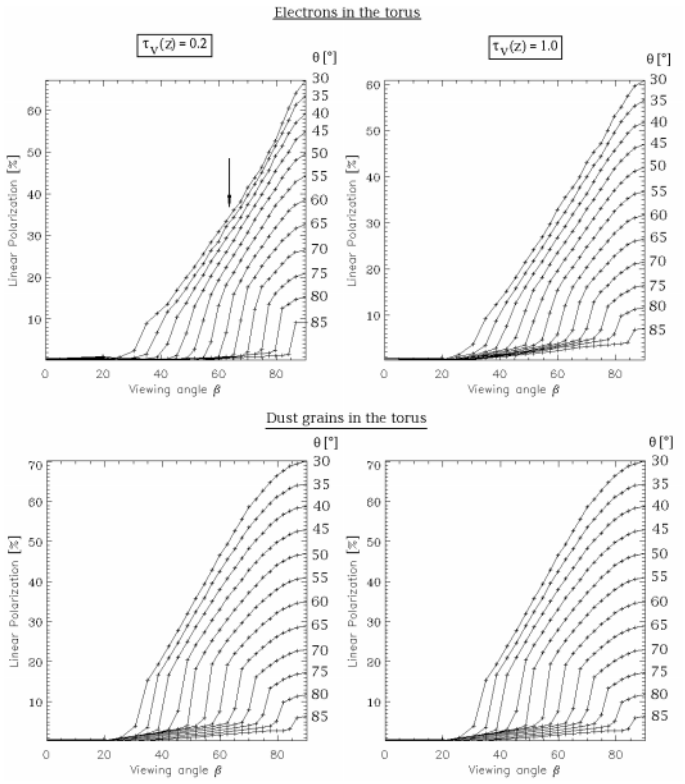

Fig. 9. Comparison between the two cases of electrons or dust grains being in the torus for two values of the optical depth. R_2/R_1=1, Dust population: ISM, λ=550nm. The arrow in the *upper left* figure shows the decrease of the P_l due to photons being scattered on the torus inner surface.

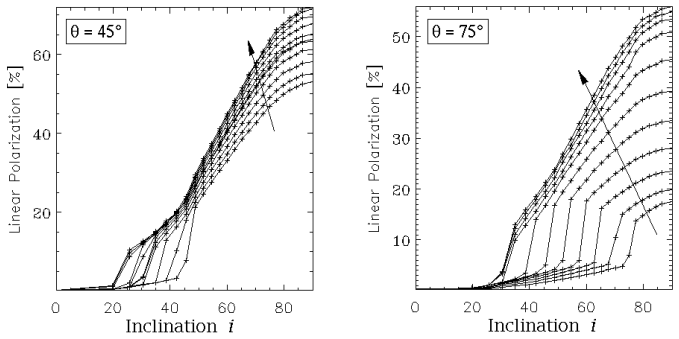

Fig. 10. Influence of a funnel on the polarization. The arrows show the shift of the curves for increasing funnel height h_f ($h_\mathrm{f}/R_2 = 0, 0.01, 0.02, \ldots, 0.10$). $\tau_\mathrm{V}(z) = 0.2$, τ_V(torus) = 1000, dust population in the torus: ISM.

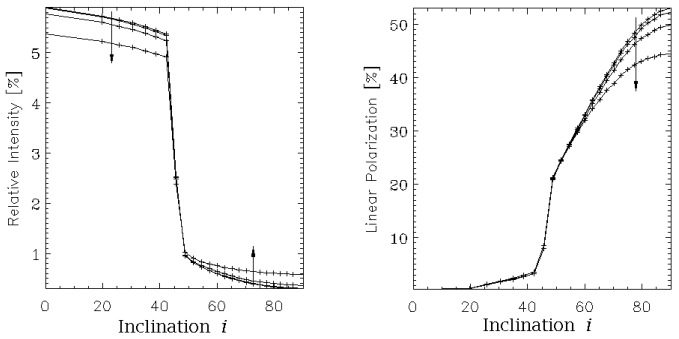

Fig. 11. Variation of the density profile in the torus: $n(r) \propto r^{-|\gamma|}$. The arrows show the shift of the curves for increasing power law exponent γ ($\gamma = 0.5, 1.0, 1.5, 2.0$). The density at the inner torus boundary (R_1) was not changed (τ_V(torus,$\gamma = 0$)=10^3). $\tau_\mathrm{V}(z) = 1$, $R_1/R_2 = 0.05$, $\theta = 45°$, λ=550nm, dust population in the torus: ISM.

Secondly, we directed our attention to those kinds of AGN models, in which the cones and – additionally – a small funnel provide the collimation of the central source radiation (see, e.g., Blandford 1985). The pre-collimation of the radiation due to the funnel leads to a decrease of the "effective" opening angle of the radiation cone ($h_\mathrm{f} > 0 \Rightarrow \theta_\mathrm{eff} < \theta$, see Fig. 3). Following the BM formalism (see Sect. 3.1.2, and Fig. 4), the polarization thereby increases with increasing funnel height (h_f). The larger the opening angle of the torus is, the larger is the difference between θ_eff and θ. This leads to a strong dependence of the polarization degree on h_f for nearly disk-like tori.

Thirdly, we varied the radial density profile in the torus. While the density $n(r)$ was constant in our previous models, we now assume a power law density distribution:

$$n(r) \propto r^{-|\gamma|}, \qquad \gamma = const. \tag{8}$$

This assumption is based on arguments of ER95 supporting the idea that the most likely geometry of a torus is that of a tapered disk with a density distribution following r^{-1} (see also Efstathiou et al. 1995 and Manske et al. 1998).

Increasing the power law exponent γ, the optical thickness of the outer region decreases. This leads to a decrease of the intensity of radiation seen under an inclination of $i < \theta$ (Seyfert 1) due to the decreased number of photons being scattered and thereby reflected on the torus surface. Because of the negligible influence of radiation that was scattered on the dusty torus (see Sect. 3.3.1), the polarization hardly changes (see Fig. 11). For inclinations $\theta < i < (180° - -\theta)$ (Seyfert 2) the intensity increases while the polarization decreases noticeably (see Fig. 11). Both effects are attributed to the decreased optical thickness of the outer torus wall.

Fourthly, we investigated the combination of electrons and dust in the cones. This configuration was proposed by Miller et al. (1991). Dust as the scattering agency for the optical continuum and broad lines is attractive because of its higher scattering efficiency per unit mass. In agreement with their observations of the active nucleus NGC 1068, it is likely that dust is present close to the nucleus anyway.

We simulated the radiative transfer in the configuration shown in Fig. 12. The cones ($\tau_\mathrm{V}(z) = 1$) contain electrons in their inner and dust (ISM population, see Sect. 2.2.2) in their outer regions. The optically thick torus is filled with dust of the ISM population, too. In agreement with the results of Manzini & di Serego Alighieri (1996) we found a strong wavelength dependence of the polarization. This result is shown in Fig. 13 for different relative extent of the electron and dust scattering regions (R_3/R_c, see Fig. 12) in the cones (opening angle $\theta = 45°$) and two viewing angles. Only dust-scattered radiation is directly ob-

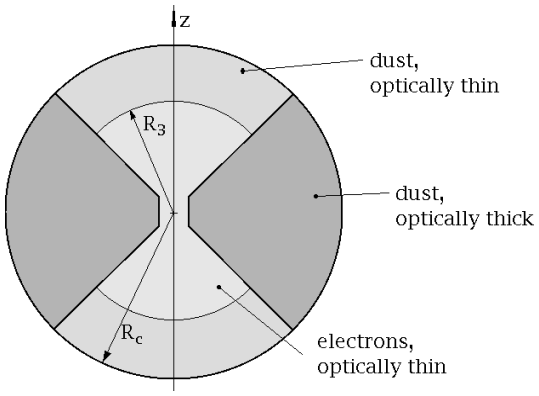

Fig. 12. Model configuration for the combination of electron and dust scattering in the cones. The density is constant in all 3 regions (inner/outer regions of the cones, torus).

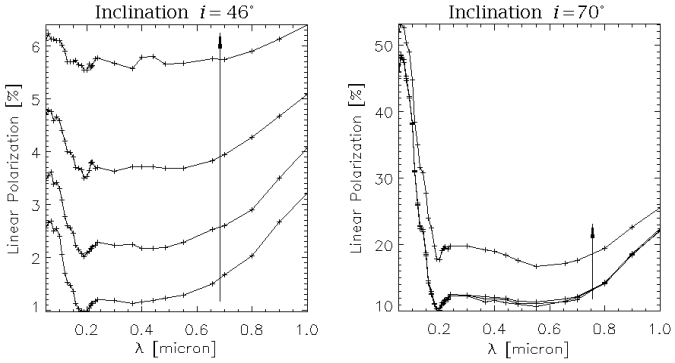

Fig. 13. Wavelength dependence of linear polarization due to the combination of electron and dust scattering in the cones. $\tau_{\rm V}(torus)$=2000, $\tau_{\rm V}(z)$=1, opening angle of the torus $\theta = 45°$, The arrows show the shift of the curves for increasing ratio $R_3/R_{\rm c}$ (see Fig. 12), $R_3/R_{\rm c}$ = 0.05, 0.1, 0.2, 0.5

served. This radiation leads to an increase of polarization with increasing $R_3/R_{\rm c}$ in the whole considered wavelength range ($0.05 \ldots 1$ μm). Hence, the difference between the polarization for different $R_3/R_{\rm c}$ ratios decreases with increasing inclination. For $i = 90°$, where the electron scattering region is fully obscured for all considered $R_3/R_{\rm c}$ ratios, this difference becomes negligible.

3.4. Extended radiation sources

In contrast to the point-like central radiation source assumed hitherto, it is necessary to investigate the influence of extended radiation sources on the observable polarization. On the one hand, the central radiation source may be extended noticeably. On the other hand, the thermal reemission of the torus has to be considered.

Manske et al. (1998) demonstrated that an anisotropically radiating central source consisting of a compact spherical component and a dust-free accretion disk surrounded by a flared dust disk gives a better agreement with observations of dust emission of AGNi seen face-on than previous models (see, e.g., ER95, Stenholm 1995). Using similar shapes of

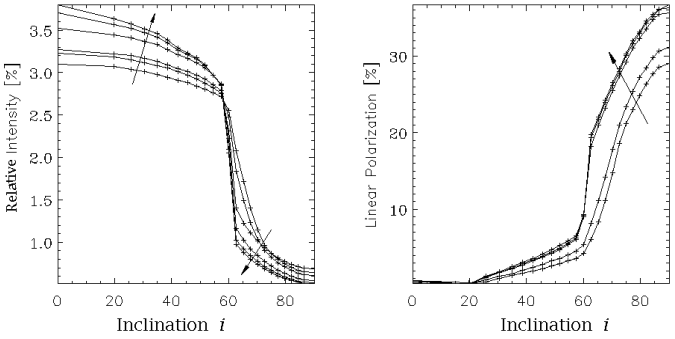

Fig. 14. Intensity and polarization resulting from the thermal reemission of the torus (surface). No central radiation source. The arrows show the shift of the curves due to an increase of ζ ($\zeta = 0, 1.0, 3.0, 4.0, 7.0, 10.0$). Dust population in the torus: ISM. Torus: optically thick at λ. $\tau(\lambda, z) = 1.0$.

the emitting central region (see Fig. 3), we found that the influence on the observable polarization is negligible (we used θ=45°, R_1/R_2=0.001 . . . 0.01, R_2=$R_{\rm c}$). Consistent with results of Cassinelli et al. (1987), neither the exact shape of the emitting region (see Fig. 3.3) nor the radial emission probability (uniform distribution of the emitters or increasing emission probability towards the centre), nor the presence or absence of scatterers in the emitting region is of importance.

Furthermore, we calculated the polarization and intensity resulting from the reemitted thermal radiation of the dusty torus (no central radiation source). The torus was assumed to be optically thick so that all test photons were emitted from its surface. The emission probability depends on the distance from the central source:

$$P_{\rm e} \propto r^{-|\zeta|} \tag{9}$$

The concentration of the emission probability close to the central source leads to an increase of the intensity seen under an inclination of $i < \theta$ (simultaneously the intensity for $\theta < i < (180° - \theta)$ decreases). For an increasing value of ζ, the polarization increases (Fig. 14). This can be explained qualitatively by the superposition of an infinite number of BM scattering configurations (see Sect. 3.1.2) being centred on the emission points of the disk, following the same spatial distribution (Eq. 9).

4. Conclusions

We presented Monte-Carlo radiative transfer simulations for various model geometries of AGNi. We tested our code for two electron density distributions and compared our results with analytical solutions.

Beginning with the most simple AGNi polarization model consisting of two diametrically opposed cones, we firstly investigated the influence of multiple scattering on the observable polarization. It was found that multiple scattering is negligible only for optical depths below ≈ 0.1, while it has a considerable influence on the radiation characteristics at higher optical depths both in the Seyfert 1 and the Seyfert 2 case.

Secondly, we added a torus to the above mentioned model. On the one hand, the torus provides the collimation of the radiation arising from a central point-like source. On the other hand, it screens the central region from the direct view ($\rightarrow$ screening effect, Seyfert 2 case). Having electrons in the cones and dust in the optically thick torus, the influence of light scattering on the torus surface was found to be marginal in contrast to the case of a torus filled with electrons. The wavelength dependence of the polarization being found for some AGNi can therefore not be explained by this model. The results for the model with dust in the optically thin cones are consistent with the observations of these AGNi. The additional presence of electrons in the inner regions of the cones increases the absolute amount of the degree of polarization. Depending on the torus size compared with the extent of the electron scattering region, the inclination of the torus may be of strong importance for the polarization degree. The inner torus radius was found to be a negligible parameter of our model (for $h_{\rm f} = 0$).

If the torus has a funnel-like inner structure ($h_{\rm f} > 0$) or a density distribution following a power law, the effective opening angle of the torus differs from the geometrical one (θ). In both cases, this leads to a considerable change of the polarization in the Seyfert 2 case. The change of the relative intensities is noticeable for both the Seyfert 1 and 2 case.

Finally, we investigated the influence of extended central radiation sources and the thermal dust re-emission of the torus on the polarization. The influence of an extended radiation source is not significant, while the polarization decreases with increasing dust re-emission intensity and with decreasing concentration of the reemitting region to the centre.

Acknowledgements. This research was supported by the DFG grant Ste 605/10 within the programme "Physics of star formation".

References

Antonucci R., 1993, ARA&A 31, 473
Antonucci R.R.J., Miller J.S., 1985, ApJ 297, 621
Brindle C., Hough J.H., Bailey J.A., et al., 1990, MNRAS 244, 577
Blandford R.D., 1985, Active galactic nuclei. Manchester University Press, p. 281
Brown J.C., McLean I.S., 1977, A&A 37, 141 (BM)
Cassinelli J.P., Nordsieck K.H., Murison M.A., 1987, ApJ 317, 290
Chandrasekhar S., 1960, Radiative Transfer. Dover, New York
Chini R., Kreysa E., Biermann P.L., 1989, A&A 219, 87
Draine B.T., Lee H.M., 1984, ApJ 285, 89
Edelson R.A., Malkan M.A., 1987, ApJ 323, 516
Efstathiou A., Rowan-Robinson M., 1995, MNRAS 273, 649 (ER95)
Efstathiou A., Hough J.H., Young S., 1995, MNRAS 277, 1134
Fischer O., Henning Th., Yorke H.W., 1994, A&A 284, 187
Fischer O., Henning Th., Yorke H.W., 1996, A&A 308, 863
Goodrich R.W., Miller J.S., 1994, ApJ 434, 82
Kartje J.F., 1995, ApJ 452, 565
Kishimoto M., 1996, ApJ 468, 606
Lawrence A., 1987, PASP 99, 309
Lawrence A., Rowan-Robinson M., Efstathiou A., et al., 1991, MNRAS 248, 91
Manske V., Henning Th., Men'shchikov A.B., 1998, A&A 331, 52
Manzini A., di Serego Alighieri S., 1996, A&A 311, 79
Miller J.S., Goodrich R.W., 1990, ApJ 355, 456 (MG90)
Miller J.S., Goodrich R.W., Mathews W.G., 1991, ApJ 378, 47
Mulchaey J.S., Wilson A.S., Tsvetanov Z., 1996, ApJ 467, 197
Pier E.A., Krolik J.H., 1992, ApJ 401, 99
Pier E.A., Krolik J.H., 1993, ApJ 418, 673
Robson E. I., Gear W. K., Brown L.M.J., Courvoisier T.J.-L., Smith M.G., 1986, Nat 323, 134
Sanders D.B., Phinney E.S., Neugebauer G., Soifer B.T., Mathews K., 1989, ApJ 347, 29
Stenholm L., 1995, ApJ 440, 597
Wolf S., Fischer O., Pfau W., 1998, A&A, submitted
Wood K., Bjorkman J.E., Whitney B., Code A.D., 1996, ApJ 461, 828
Young S., Hough J.H., Axon D.J., Bailey J.A., Ward M.J., 1995, MNRAS 272,513